Multipole magnets for the HIAF fragment separator using the Canted-Cosine-Theta (CCT) geometry

Multipole magnets for the HIAF fragment separator using the Canted-Cosine-Theta (CCT) geometry

Wei Wu[1], Yu Liang[1], Lun-Cai Zhou[1], En-Ming Mei[1], Dong-Sheng Ni[1], Shi-Jun Zhen[1], Xian-Jin Ou[1], and Wen-Jie Yang[1]

[1]Institute of Modern Physics, Chinese Academy of Sciences, Lanzhou, 730000, China

E-mail: wuwei@impcas.ac.cn

Abstract. The fragment separator of the HIAF (High Intensity Heavy Ion Accelerator Facility) project called HFRS requires quadrupoles with high gradients (11.4 T/m) and large bores (320 mm in diameter). The iron dominated magnets with superconducting coils have been widely used in the similar facilities such as A1900, BigRIPS, Super-FRS and RISP with the advantages of low request for coils installation precision, simple fabrication and low cost, but they have large cold mass and helium containment, which result in long time cooling down and high pressure rise during a quench. In addition, due to iron saturation, it is hard to guarantee on the field quality in the operated field range. A new coil dominated design based on the Canted-Cosine-Theta geometry is presented for HFRS, which is expected to overcome these problems. The design superimposes several layers of oppositely wound helical windings to generate high quality quadrupole. Sextupole, octupole and steering dipole can also be easily integrated to reduce the length of cryostat. This paper reports the detailed design of HFRS multiplets based on the CCT concept and the construction of a subscale prototype.

1. Introduction

The **H**igh **I**ntensity **A**ccelerator **F**acility is a new project to pursue nuclear physics research and is under construction at the Institute of Modern Physics in China [1]. As shown in Fig. 1, it consists of a 45 GHz superconducting ECR ion source, a superconducting Linac, a fast cycling booster ring, a fragmentation separator and a spectrometer ring. The fragmentation separator of HIAF called HFRS is an important connection between BRing and SRing. It is used to produce, separate, purify, and identify the desired exotic nuclei. The field rigidity is 25 T • m. It has a big beam acceptance of $\pm$160 mm. For similar facilities, such as A1900 [2], BigRIPS [3], [4], SuperFRS [5] and RISP [6], to meet the magnetic field requirement within a large aperture, the superferric design with cold iron have been widely used. They are easy to fabricate and wind, while their coils require lower positioning precision. But because of the iron saturation, it is hard to achieve good field quality at both low and high field with the superferric design. And large cold mass also brings new challenges, such as long-time cooling-down, high pressure during a quench and difficulties of supporting and alignments. Air-core type magnets have the advantages of light weight and good field linearity and are used in BigRIPS as the first element near the target to lower the radiation heat load [7]. Walstrom type coil with better field quality are used in the S^3 device of SPIRAL2 project [8], [9]. But their magnetic field are more sensitives to coil positioning error and they are difficult to fabricate and wind.

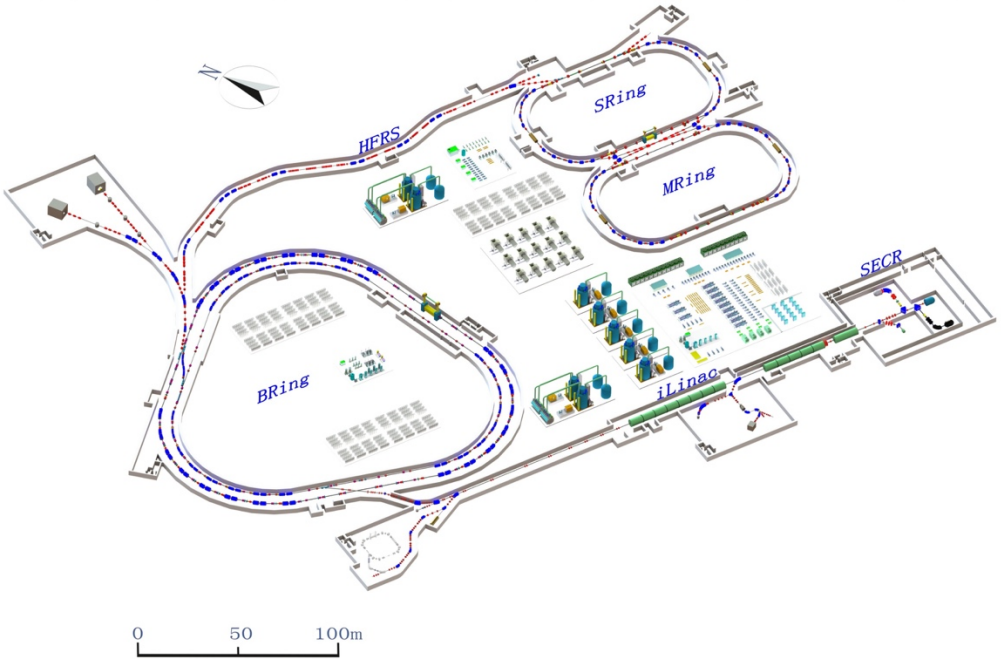

Figure 1. Layout of HIAF project.

2. Canted-Cosine-Theta magnet

The basic idea of **C**anted-**C**osine-**T**heta was firstly published by D. I. Meyer and R.Flasck in 1970 [10]. As shown in Fig. 2, by the superposition of two oppositely tilted solenoids with respect to the bore axis, the azimuthal component of the magnetic field is cancelled, and the high-quality dipole field can be generated.

Higher order multipole fields can also be obtained by superimposed current with an z direction oscillation as shown in following equations. For example, n=2 produces a quadrupole field as shown in Fig. 3, and so forth.

$$x(\theta) = R \cdot \cos(\theta) \tag{1}$$

$$y(\theta) = R \cdot cos(\theta) \tag{2}$$

$$z(\theta) = \frac{h}{2\pi}\theta + \sum_n A_n sin(n\theta + \varphi_n) \tag{3}$$

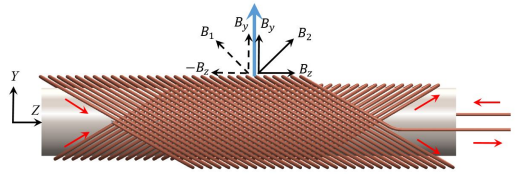

Figure 2. Conceptual view of CCT dipole windings.

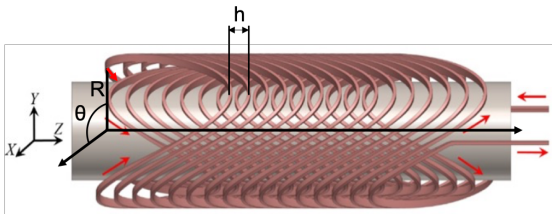

Figure 3. Conceptual view of CCT quadrupole windings.

Because of its flexibility and field quality in comparison to convectional superconducting magnets, CCT magnet gained new traction. Meinke *et al*. described their studies in a series of publications [11–14]. More recently, Caspi et al. have successfully developed a series of CCT dipole prototypes with NbTi and Nb3Sn [15-17] and also presented a Proton gantry design based on CCT coils [18]. At CERN, for Hi-Lumi LHC orbit correctors, the CCT solution was finally retained for the advantages of easier assembly and lower cost, compared with the classical Cosine-Theta design [19]. It was also an

option for the 16-T FCC-hh main dipole which is under development in PSI [20]. In short, the CCT coil is at a balance point between field quality and cost, thus, our HFRS complex also chose the CCT as baseline solution.

3. Magnetic design

In Fig. 4 the layout of HFRS is shown. A total of 39 superconducting singlets are grouped into 13 triplets and cryostat modules. Fig. 5 shows a typical lattice of HFRS singlet, consisting of three quadrupoles with different effective length, sextupole, octupole and steering dipole.

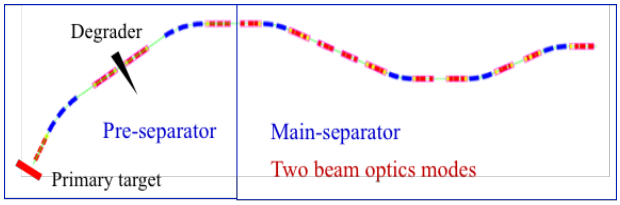

Figure 4. Layout of HFRS.

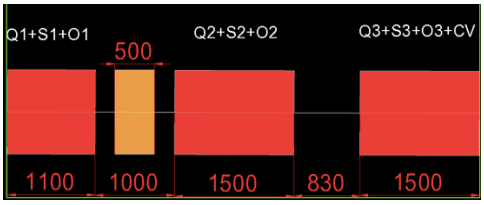

Figure 5. A typical lattice of HFRS singlet.

The usable magnet aperture is 320 mm and the field gradient is 11.43 T/m. Field requirements for quadrupole, sextupole and octupole field are summarized in Table 1. In addition, dipole coils are used for two directions' steering corrections. The quadrupole coil, which experience the highest field, is the most demanding coil. Thanks to the good features of CCT coil, octupole, quadrupole, sextupole and dipole fields can be nested to reduce the mechanical length of the cryogenic modules.

Table 1. Magnet Specifications.

	Quadrupole	*Sextupole*	Octupole
Aperture	320 mm	320 mm	320 mm
Gradient	11.43 T/m	30 T/m^2	105 T/m^3
Effective length	0.8/ 1.1/1.5 m	0.8/ 1.1/1.5 m	0.8/ 1.1/1.5 m
Field quality	$< \pm 8 \cdot 10^{-4}$	$< \pm 5 \cdot 10^{-4}$	$< \pm 5 \cdot 10^{-4}$

3.1. Comparison of different conductor placement methods

For complicate coil like CCT, two types of conductor placement methods can be considered. First is the **direct placement with adhesive**, such as BNL's direct winding technology [21] with ultrasonic adhesive system. Recently, techniques that thermally embedded wire into thermal plastic material have also been applied in the fabrication of RF smart card coils and 3D printing of electromechanical devices [22]. But this method requires special equipment.

Another is conductor placement in grooves. Superconducting wires or cables can be placed into machined grooves from metal or composite mandrel. With cable, the CCT magnet's operation current is high and its inductance is low, which is suitable for powering in a string of magnets. With wire, its operation current is low while the inductance is high, which is a good choice for magnets powered with standalone converters. But it needs more mandrels if the grooves can only accommodate one wire. More mandrels mean higher cost, in order to lower the cost, CERN winds several insulated wires (2 x 5) into one groove and then connects them in series as shown in Fig. 6 (a). This method could be named coil placement in grooves. In order to improve the positioning accuracy, simplify the winding process and eliminate the insulation thickness of each wire, we come up with a variant that puts mini round cable with 7 insulated wires into groove as shown in Fig. 6 (b). Compared with CERN's solution, this design has more flexibility of insulation design that wire insulation is for turn to turn and cable insulation is for ground. Due to the transposition of wires, the coupling loss can be reduced.

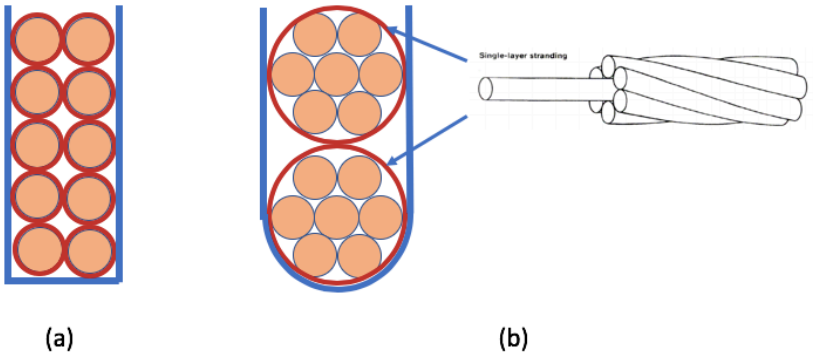

Figure 6. Conceptual drawing of coil placement in grooves and its variant with mini round cable.

3.2. Conductor selection and insulation system

In order to reduce the power supply and current leads costs, operational current lower than 500 A is chosen. When the peak field is about 3.5 T, the Nb-Ti wire is selected. Its specifications are summarized in Table 2. In order to withstand high radiation dose while maintaining voltage insulation levels > 1 kV, polyimide coating is used. The mini round cable is stranded by 7 insulated wires and wrapped with two layers of polyimide tapes for insulation (see Table 3). The voids between two adjacent cable can be filled with copper alloy wire as heater and glass fiber, then vacuum impregnated with CTD101K resin system. The impregnation also provides a support for the cables inside the grooves.

Table 2. NbTi Superconductor Specifications.

	Units	
Wire diameter	mm	0.85
Diameter with insulation (polyimide coating 0.025mm)	mm	0.90
Number of NbTi filaments		630
Filament diameter	μm	22
Cu RRR		>100
n-value		>30
Cu/Sc		1.3
Ic@4.2K 4 T	A	>750

Table 3. NbTi Superconductor Specifications.

	Units	
Number of strands		6+1
Cable diameter	mm	2.70
Cable diameter with insulation (Polyimide tape wrapped)	mm	2.80

3.3. CCT coil design of HFRS singlet

For each singlet, a set of multipole coils are nested concentrically with their mandrels. In order to reduce the cold mass and transfer function non-linearity, room temperature iron yoke outside of cryostat is used. The coils are designed to generate lower field which can be enhanced by the iron yoke. Table 4 list the design parameters of quadrupole and sextupole CCT coils with the effective length of 0.8 m.

Table 4. Overview of Magnet Parameters.

Characteristics	Quadrupole	Sextupole
Gradient Field	10 T/m	30 T/m^2
I/wire	440 A	330 A
Layers	2×(6+1)	1×(6+1)
CCT skew angle	30°	40°
Turns per layer	66	64
ID of mandrel	420 mm	453.2 mm
Pitch	12.2 mm	12.6 mm
Groove size	2.8mm×5.8mm	2.8mm×3mm
Conductor length	6.4 km	3.4 km
Bpeak	3.5 T	3.0 T
Io/Iss	54%	37.5%

The quadrupole and sextupole coils are modelled in OPERA-3D as shown in Fig. 7 and the peak field located in the inner quadrupole coil is about 3.5 T as shown in Fig. 8. The octupole (Fig. 9) and steering dipole coils (Fig. 10) are designed in the pattern of discrete Cosine-Theta coil and will be mounted inside the quadrupole coil and outside the sextupole coil, respectively.

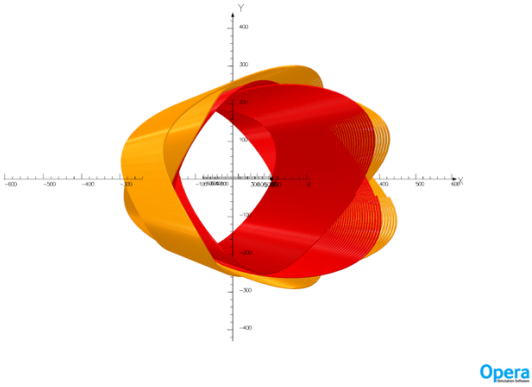

Figure 7. CCT coil model created by OPERA.

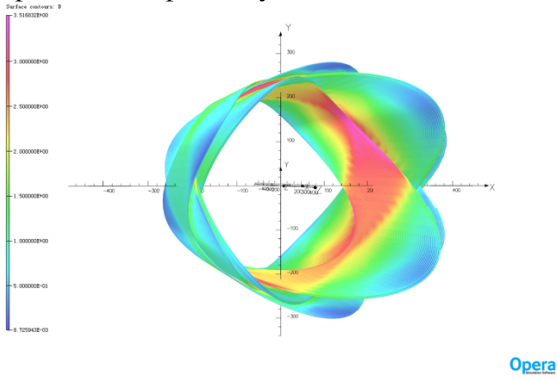

Figure 8. B map of the CCT coil model.

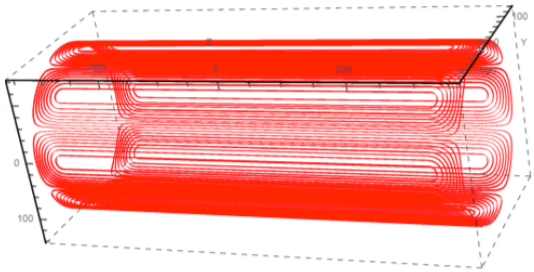

Figure 9. Octupole coil.

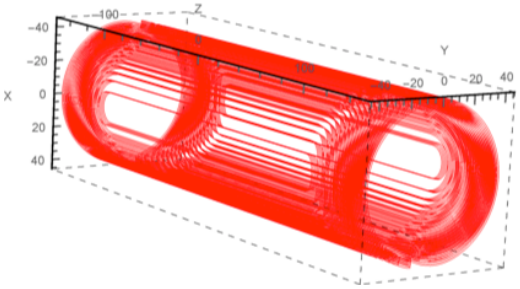

Figure 10. Steering dipole coil.

4. Mechanical design

The coil winding is embedded in aluminum alloy coil formers with CNC machined slot. The machined formers are hard anodized for insulation. As shown Fig. 11, the singlet assembly is comprised of two formers for quadrupole and two formers for sextupole, GFRP (Glass-Fiber-Reinforced Plastic) former for steering dipole, aluminum outer support tube, two end plates, and two joint boxes for quadrupole and sextupole coils' connections. In order to guarantee the field quality, the positional accuracy of the

grooves need to be controlled within 0.05 mm. According to the preliminary error analysis, the tolerance of concentricity of four formers is within 0.1 mm. The assembly is then vacuum impregnated with CTD101K resin. Finally, three singlets are inserted into a central stainless bobbin as triplets. The bobbin also serves as a part of the helium vessel.

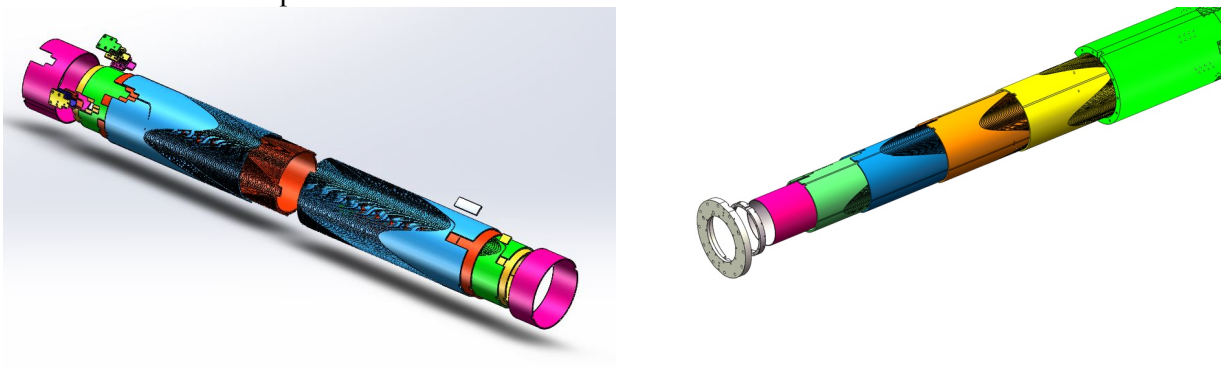

Figure 11. 3D drawing of the singlet assembly.

5. Subscale model coil

In order to study the feasibility of the CCT design. We designed and fabricated a subscale quadrupole coil (see Fig. 12). As listed in Table 5, the field gradient is 40 T/m within a 60mm cold bore. The effective length is 160 mm. The NbTi conductor as described in Table 6 was used. The groove size is 2 x 5 mm for ten turns of conductor as shown in Fig. 6 (a). Same method of coil placement in grooves as CERN's was adapted. Figure 13 shows the process of winding 10 turns of wires into grooves. After winding, assembly, splicing, vacuum impregnation and wiring, the coil was successfully energized to design current without any quench. Fig. 14 shows the measured radial field increased linearly with operated current.

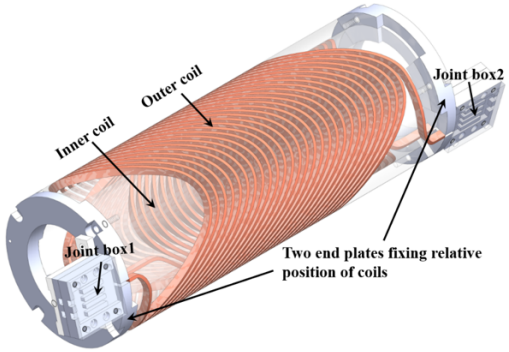

Figure 12. 3D drawing of the subscale model coil.

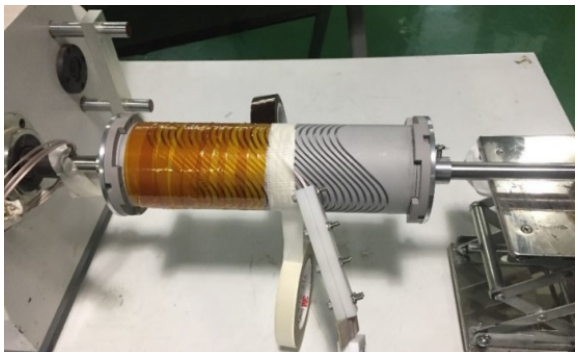

Figure 13. Winding process of the subscale quadrupole coil.

Table 5. Parameters of Subscale Model Coil.

Parameter	Unit	Value
Gradient	T/m	40
Effective length	Mm	160
Operation current	A	400
Winding pitch	mm	6
Tilt angle	Deg	45
Inductance	mH	10
Aperture	mm	60
Good field	mm	± 20

Table 6. Specifications of the Superconductor Used in the Subscale Model Coil.

Wire type	Monolith
Insulation	Formvar + Polyester braid
Bare size	Φ 0.72 mm
Insulated size	Φ 0.77 mm (Formvar)
	Φ 0.9 mm±5 μ m (Polyester braid)
Cu/SC	1.3:1
RRR (293 K/10 K)	> 100
Ic (6 T, 4.2K)	442.7 A

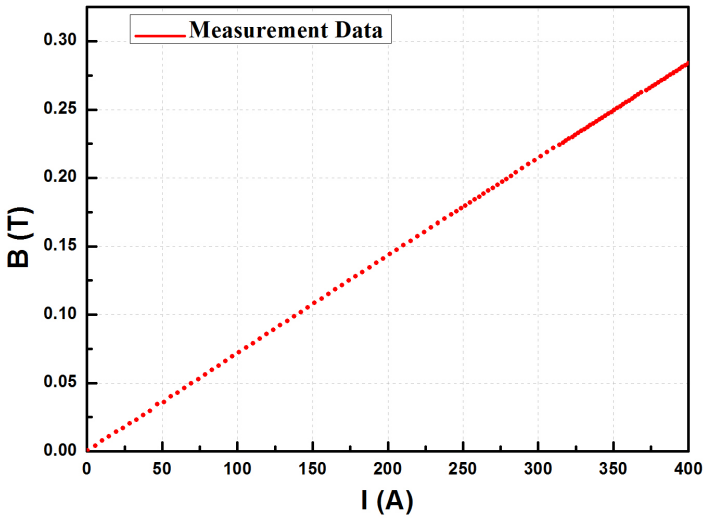

Figure 14. Measured transfer function (Br at radius of about 7 mm).

6. Project planning

IMP plans to fabricate and test a model singlet with nested quadrupole, sextupole, octupole and steering dipoles by the June of 2019. The effective length is 0.8 m and the bore diameter are 200 mm. And then the full-size prototype singlet and triplets will be built by the middle of 2020. Totally 13 sets of multiplets need to be produced and tested before the end of 2023.

7. Conclusion

The novel CCT geometry coil structure has been adapted to the multiple magnets design of HFRS spectrometer. It reduces significantly size, weight of cold mass, cryogenic system and magnet installation requirements and cost of fabrication and operation. However, further error analysis of field quality, quench simulation and stress analysis are now on going to ensure the field quality and safety operation of the full-size magnets.

Acknowledgments

The authors would like to express their sincere acknowledge to Prof. Lucio Rossi (CERN), Prof. Glyn Kirby (CERN), and Prof. Shlomo Caspi's (LBNL) for their comments and useful suggestions.

The work is supported by the National Natural Science Foundation of China (Grant No. 11575266).

References

[1] Yang, J. C., Xia, J. W., Xiao, G. Q., Xu, H. S., Zhao, H. W., Zhou, X. H., et al. (2013). High Intensity heavy ion Accelerator Facility (HIAF) in China. *Nuclear Inst. and Methods in Physics Research*, B, **317**, 263–265.

[2] Zeller, A. F., DeKamp, J. C., Johnson, D., Marti, F., Morrissey, D. J., Sherrill, B. M., et al. (1998). Magnetic elements for the A1900 fragment separator at the NSCL. *Advances in Cryogenic Engineering*, **43**, 245–252.

[3] Kubo, T. (2003). In-flight RI beam separator BigRIPS at RIKEN and elsewhere in Japan. *Nuclear Inst. and Methods in Physics Research*, B, **204**, 97–113.

[4] Kusaka, K., Kubo, T., Mizoi, Y., Yoshida, K., Yoshida, A., Tominaka, T., et al. (2004). Prototype of superferric quadrupole magnets for the BigRIPS separator at RIKEN. *IEEE Transactions on Appiled Superconductivity*, **14**(2), 310–315.

[5] Leibrock, H., Floch, E., Moritz, G., Lizhen Ma, Wei Wu, Ping Yuan, et al. (n.d.). Prototype of the Superferric Dipoles for the Super-FRS of the FAIR-Project. *IEEE Transactions on Appiled Superconductivity*, **20**(3), 188–191.

[6] Zaghloul, A., Kim, D., Kim, J., Kim, M., Kim, M., Yun, C., & Kim, J. (2015). Design of large aperture superferric quadrupole magnets for an in-flight fragment separator (Vol. **1573**, pp. 416–421). Presented at the ADVANCES IN CRYOGENIC ENGINEERING: *Transactions of the Cryogenic Engineering Conference* - CEC, AIP Publishing LLC.

[7] Kusaka, K., Kubo, T., Yano, Y., Kakutani, N., Ohsemochi, K., Kuriyama, T., et al. (n.d.). An Air-Core Type Superconducting Quadrupole Triplet for the BigRIPS Separator at RIKEN. *IEEE Transactions on Appiled Superconductivity*, **18**(2), 240–243.

[8] Déchery, F., Drouart, A., Savajols, H., Nolen, J., Authier, M., Amthor, A. M., et al. (2015). Toward the drip lines and the superheavy island of stability with the Super Separator Spectrometer S3. *The European Physical Journal* A, **51**(6), 66.

[9] Walstrom, P. L. (2004). Soft-edged magnet models for higher-order beam-optics map codes. *Nuclear Inst. and Methods in Physics Research*, A, **519**(1-2), 216–221.

[10] Meyer, D. I., & Flasck, R. (1970). A new configuration for a dipole magnet for use in high energy physics applications. *Nuclear Inst. and Methods*, **80**(2), 339–341.

[11] Goodzeit, C. L., Ball, M. J., & Meinke, R. B. (2003). The double-helix dipole - a novel approach to accelerator magnet design. *IEEE Transactions on Appiled Superconductivity*, **13**(2), 1365–1368.

[12] R. B. Meinke et al.(2003). Superconducting double-helix accelerator magnets, in *Proc. Particle. Acc. Conf.*, pp. 1996–1998.

[13] Gavrilin, A. V., Bird, M. D., Keilin, V. E., & Dudarev, A. V. (2003). New concepts in transverse field magnet design. *IEEE Transactions on Appiled Superconductivity*, **13**(2), 1213–1216.

[14] Gavrilin, A. V., Bird, M. D., Bole, S. T., & Eyssa, Y. M. (2002). Conceptual design of high transverse field magnets at the NHMFL. IEEE Transactions on Appiled Superconductivity, 12(1), 465–469.

[15] Caspi, S., Brouwer, L. N., Lipton, T., Hafalia, A., Jr, Prestemon, S., Dietderich, D. R., et al. (2015). Test Results of CCT1—A 2.4 T Canted-Cosine-Theta Dipole Magnet. *IEEE Transactions on Appiled Superconductivity*, **25**(3), 1–4.

[16] Caspi, S., Borgnolutti, F., Brouwer, L., Cheng, D., Dietderich, D. R., Felice, H., et al. (2014). Canted–Cosine–Theta Magnet (CCT)—A Concept for High Field Accelerator Magnets. *IEEE Transactions on Appiled Superconductivity*, **24**(3), 1–4.

[17] L. Brouwer, Canted-cosine-theta superconducting accelerator magnets for high energy physics and ion beam cancer therapy, Ph.D. dissertation, Univ. California, Berkely, CA, USA, 2015, ISBN 978-83-7814-491-5.

[18] S. Caspi, D. Arbelaez, L. Brouwer, D. Dietderich, R.Hafalia, D. Robin, A. Sessler, C. Sun, and W. Wan(2012), Progress in the Design of a Curve Superconducting Dipole for a Therapy Gantry, *Proceedings of IPAC2012*, New Orleans, Louisiana, p. 4097-4099.
[19] G. A. Kirby et al.(2017). Hi-Lumi LHC Twin-Aperture Orbit Correctors Magnet System Optimisation. *IEEE Transactions on Applied Superconductivity*, **27**(4), 1-5.
[20] B. Auchmann et al.(2018). Electromechanical Design of a 16-T CCT Twin-Aperture Dipole for FCC. I*EEE Transactions on Applied Superconductivity*. 28(3), 1-5.
[21] Parker, B., Anerella, M., Escallier, J., Ghosh, A., Jain, A., Marone, A., et al. (2007). BNL Direct Wind Superconducting Magnets. *IEEE Transactions on Appiled Superconductivity*, **22**(3), 4101604–4101604
[22] Saari, M., Cox, B., Richer, E., Krueger, P. S., & Cohen, A. L. (2015). Fiber Encapsulation Additive Manufacturing: An Enabling Technology for 3D Printing of Electromechanical Devices and Robotic Components. *3D Printing and Additive Manufacturing*, **2**(1), 32–39